Key Engineering Materials
ISSN: 1662-9795, Vol. 1049, pp 75-87
doi:10.4028/p-Nz4ICc

Submitted: 2026-01-19
Revised: 2026-02-16
Accepted: 2026-03-02
Online: 2026-04-15

Hybrid Numerical and Data-Driven Modelling for Defect Prediction in Screw Press Hot Bulk Forging of the EN AW-6060 Part

Artem Alimov[1,a*], Yuyao Jiang[2,b], Markus Gardill[2,c] and Sebastian Härtel[1,d]

[1]Chair of Hybrid Manufacturing, Brandenburg University of Technology Cottbus-Senftenberg, Konrad-Wachsmann-Allee 17, 03046 Cottbus, Germany

[2]Chair of Electronic Systems and Sensors, Brandenburg University of Technology Cottbus-Senftenberg, Siemens-Halske-Ring 14, 03046 Cottbus, Germany

[a*]alimov@b-tu.de, [b]jiangyuy@b-tu.de, [c]gardill@b-tu.de, [d]haertel@b-tu.de
(*corresponding author)

Keywords: FEM modelling, data-driven modelling, hot bulk forging, defect prediction.

Abstract. Numerical simulation, particularly through the Finite Element Method (FEM), is widely applied in the design and optimization of metal forming processes. However, certain real-process effects are not fully captured by numerical models alone, creating a need for complementary data-driven approaches. This study presents a hybrid modelling framework that integrates FEM simulations with machine-data-based predictive modelling to improve defect prediction in hot forging. Experimental data were collected from automated forging trials on an SMS SPPE 6.3 screw press equipped with position, force, strain, acceleration, and frame-deflection sensors. A series of trials with varied process parameters enabled the development of a data-driven classification model for detecting the "underfilling" defect. In parallel, the FEM model was refined by incorporating additional real-process phenomena, including ram tilt, press-frame deflection, and air entrapment in die cavities. The combined approach significantly enhanced defect prediction accuracy and provided deeper insight into the mechanisms driving defect formation. These results demonstrate the effectiveness of hybrid numerical–data-driven modelling for improving the robustness of metal forming process design.

Introduction

Numerical Modelling of metal forming processes is widely used in modern industry, both in the design of new processes and in the analysis and improvement of existing ones [1]. The current state of Modelling techniques enables virtually all significant factors affecting the quality of forgings to be taken into account [2]. The use of inverse analysis significantly improves the accuracy of models used in simulation [3] and allows the process optimization [4]. However, a number of phenomena are either not considered at all or are considered only in rare cases. Firstly, the metal forming process in simulation is most often assumed to be deterministic, without considering stochastic effects and uncertainties [5]. This can lead to defect formation during real forging, even though the simulation predicted a defect-free process. Another significant factor may be the discrepancy between the real behavior of the forging machine and the idealized equipment model used in the simulation [6]. For example, in most simulations, the elastic deflection of the forging machine is usually neglected and it is considered to be perfectly rigid [7]. In the case of force-bound forging machines, this can lead to insufficient forming or increased forming force, while in energy-bound forging machines, it leads to a loss of energy and, similarly, to defects [8]. In order to implement the real forging machine behavior, the experimental data should be at first acquired and then analyzed. One of possible ways to acquire data from forging machine is to use modern industrial sensor technology, especially non-contact radar-based sensors [9]. The obtained dataset can be further analyzed using methods of data-driven modelling [10]. Machine learning is presently one of the main approaches used in data-driven modelling and as a branch of artificial intelligence offers the widest opportunities for data analysis, both experimental [11] and synthetic [12] , as well as for creating models and optimizing processes. The application of hybrid modeling by combining the physics-based modeling together with real

experimental data allows to utilize the advantages of both methods and to improve the efficiency and accuracy of prediction [13]. This makes it possible to reduce the gap between simulation and reality, which is one of the main quality assurance challenges in metal forming today.

The most common defects occurring during metal forming are underfills and folds [14]. The causes of these defects are most often incorrect metal flow due to improper design or unfavorable process conditions, as well as an insufficient amount of metal due to the low precision of the raw material or its cutting [15]. Underfilling can also occur due to increased resistance to metal flow in the die cavity caused by air or lubricant trapped in these cavities.

This work continues our previous research, devoted to integrating uncertainties into FEM simulations and forging process robustification [12] and outlines a combined modelling approach that brings together FEM simulations and data-driven methods to improve prediction and detection of underfilling defects in hot forging. The experimental data came from a series of automated tests carried out on an SMS SPPE 6.3 screw press equipped with advanced data acquisition system. By intentionally varying several process parameters during the trials, we were able to build a classification model capable of recognizing when underfilling occurs. In parallel, the FEM model was adjusted to reflect conditions that appear in actual production, such as slight ram tilting, deformation of the press frame, and pockets of air trapped in die cavities. Bringing these two parts together – numerical Modelling and data-driven analysis – resulted in noticeably better defect-prediction performance and provided a deeper understanding of the factors leading to defect formation. Overall, the results show that combining numerical simulations with real-process data can make the design of metal forming operations more reliable and more resilient.

Materials and Methods

Materials. Workpieces were produced from EN AW 6060 (AlMgSi, DIN 3.3206) D35x6000 mm bars provided by Gemmel Metalle GmbH. The workpieces were cut with industrial bandsaw MEBAswing 405 DG and then turned to the final dimensions using Colchester Student VS lathe. The chemical composition is presented in Table 1.

Table 1. The chemical composition of used EN AW 6060

Element	Mg	Si	Fe	Cu	Mn	Ti	Zn	Al
Nom.	0.35-0.60	0.30-0.60	0.10-0.30	< 0.10	<0.10	<0.10	<0.15	Bal.
Fact.	0.436	0.596	0.186	0.004	0.012	0.015	0.003	

The forging dies were machined from hot work tool steel X37CrMoV5-1 (DIN 1.2343) provided by MARKS GmbH and subsequently vacuum hardened and tempered to the final hardness of 45…48 HRC.

Automated screw press hot bulk forging. The forged part (Figure 1) represents a combination of a cylindrical-walled head and an elongated cruciform element.

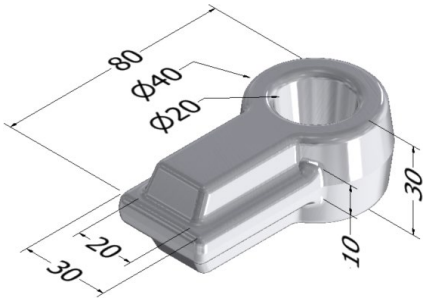

Fig. 1. Forged part

This geometry consists of elements typical for hot forged parts and allows for high-accuracy analysis of how deviations in forging process parameters affect defect formation due to the low fillability of the die cavities. The workpiece is a cylinder. Forging was carried out on an automated press shop

based on an SMS SPPE 6.3 screw press equipped with two robotic manipulators for transporting workpieces and lubricating dies. A scheme of the automated press shop is shown in Figure 2.

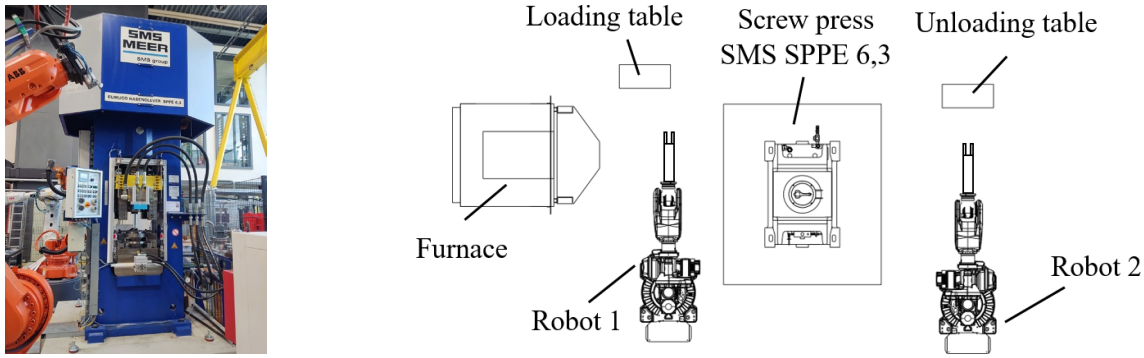

Fig. 2. SMS SPPE 6.3 screw press (a) and test setup for automated forging (b)

Robot 1 picks up the workpiece from the loading table and places it into the furnace. If necessary, the furnace chamber can be filled with a protective gas. After holding the workpiece at the specified temperature for the required time, Robot 1 removes it from the furnace, places it in the die, and sends a signal to initiate forging. The press performs forging according to the specified program, with the required number and energy of blows, after which the workpiece is ejected from the die cavity.

Robot 2 then picks up the workpiece and lubricates the dies by spraying using a lubrication head mounted on its arm. Next, the robot transports the workpiece to the unloading table and returns to its home position. The cycle is then repeated.

The forging process is carried out in a fully automated mode, which eliminates errors and inaccuracies associated with manual operation and handling of the workpiece.

Hybrid Numerical and Data-Driven Modelling. The hybrid approach to numerical and data-driven Modelling used consists of two complementary components. The first involves automated FEM simulations to generate a representative dataset followed by its analysis using machine learning methods. The second component includes the acquisition of experimental data, feature extraction, and subsequent linear discriminant analysis. Together, these elements enable effective defect prediction and detection. The approach diagram is shown in Figure 3.

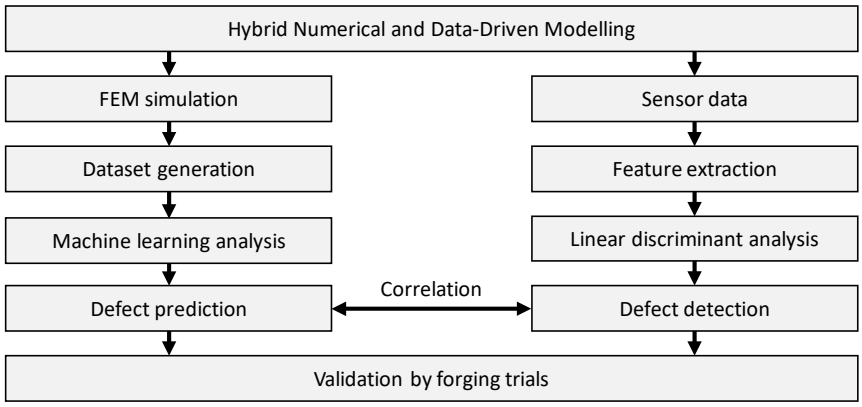

Fig. 3. Approach to hybrid numerical and data-driven modelling.

Data acquisition system. The SMS SPPE 6.3 screw press equipped with a comprehensive data acquisition system that includes of the following sensors:

- Four magnetostrictive position sensors for determining the spatial position of the ram;
- Four magnetostrictive sensors for measuring deflection at the corners of the press frame;
- A system of five radar-based position sensors for monitoring both ram motion and frame elongation;

- An accelerometer mounted on the press ram;
- Two strain gauge force sensors mounted on the press frame columns;
- Four local piezoelectric sensors integrated into the bottom die.

Data of the sensors except radar-based position sensors is collected by Consenses EdgeSenses data acquisition system. Detailed information on the architecture of the radar sensor network is provided in the article by Jiang et al. [9].

FEM Simulation. Automated API-driven FEM simulations were carried out using the commercial FEM software QForm UK 12.0.1 (www.qform3d.com) in a general forming module. A detailed description of the simulation methodology and the material properties, as well as process parameters, used in the simulations, are provided in the paper by Alimov et al. [12]. In order to reduce computation time, the process was considered symmetrical with respect to the YOZ plane, and only one half of the workpiece was simulated (Figure 4).

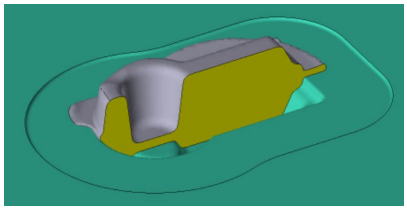

Fig.4. Workpiece symmetry used in the simulation

Consideration of trapped air in die cavities. Air, trapped in deep die cavities can cause underfilling and should therefore be modelled. The simulation of trapped air was performed using the brand-new feature of QForm UK 12.0.1. This approach will be presented in detail at the Metalforming 2026 conference [16]. The method involves simulation of metal flow using the finite element method to analyze the evolution of the flow front. Regions susceptible to gas entrapment are automatically identified as cavities where the advancing metal encloses isolated gas pockets (Figure 5). The internal gas pressure in each cavity is estimated using adiabatic compression law, allowing quantitative assessment of the risk of underfill defects.

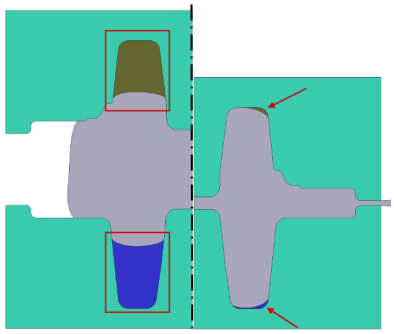

Fig. 5. The principle of trapped air simulation

The parameters used in simulation of trapped air are shown in Table 2.

Table 2. Trapped air simulation parameters

Parameter	Value
Max. pressure in cavity [MPa]	300
Max. pressure growth by solve step [%]	50
Max. surface area to volume ratio	4
Adiabatic index	1.4
Trapped air initial gauge pressure [MPa]	0

Consideration of press frame deflection. Press frame deflection was considered by using the spring-loaded bottom die. Part of the blow energy is thus spent on the elastic compression of this spring, analogous to the deflection of the press frame. Only the spring stiffness was varied during the simulation, and the initial compression was zero, since the press frame does not have tie rods.

Consideration of press ram tilting. Press ram tilting was considered only within the workpiece symmetry plane by rotating the top die in this plane at a certain angle, since the position of the workpiece in the direction perpendicular to the workpiece symmetry plane does not change due to stable placement in the die cavity and the forces are being balanced due to the symmetry.

Design of simulations and experiments. A dataset of 120 simulations for further analysis by means of machine learning was created using Latin hyper cube sampling with automated FEM-simulations. A random forest was used to analyze the effect of process parameter variation of defect formation. The effect of the individual features on the underfill defect formation was analyzed using the explainable method SHapley Additive exPlanations (SHAP). For a detailed description of the implementation and methods used, please refer to [17].

Variable process parameters and their ranges used in numerical modelling are presented in Table 3. The experimental investigations were carried out under defined process conditions. To produce defect-free forged parts, a reference parameter set was used. Under these conditions, a total of 27 defect-free forged parts were manufactured. To deliberately generate defective forged parts, two defect-inducing parameter sets with workpiece displacement OY of +10 mm and -10 mm while keeping another parameter as reference were applied, resulting in the production of 11 and 12 defective forged parts, respectively.

Table 3. Variable process parameters and their ranges used in simulations

Parameter	Reference value	Minimal value	Maximal value
Initial workpiece temperature, °C	480	440	480
Workpiece diameter, mm	35	31	38
Workpiece length, mm	72	68	74
Workpiece displacement OY, mm	0	-10	10
Die 1 rotation YOZ, °	0	-0.1	0.1
Die 2 spring stiffness, MN/mm	Inf.	1	24

Linear Discriminant Analysis. Linear Discriminant Analysis (LDA) [18,19] is a supervised dimensionality reduction technique that allows to find a linear projection of the feature space in which class separability is maximized. It is based on Fisher's discriminant criterion, whose objective is to determine a projection that maximizes the ratio of between-class scatter to within-class scatter. Let S_b and $S_w$denote the between-class and within-class scatter matrices, Fisher' s criterion can be formulated by maximizing the following equation

$$J(W) = \frac{|W^T S_b W|}{|W^T S_w W|}, \tag{1}$$

where W is the LDA solution that contains up to $c-1$ eigenvectors, with c being the number of classes. This can be solved as a generalized eigenvalue problem

$$S_b w_i = \lambda_i S_w w_i, \tag{2}$$

where $w_i \; and \; \lambda_i$ are respectively the i-th generalized eigenvector and eigenvalue of S_b with respect to S_w.

The signals from each sensor within the time interval from 0.4 s to 0.6 s were extracted and perform the aforementioned feature extraction. During this period, the workpiece is in contact with the die. LDA was implemented using the scikit-learn library in Python.

Feature extraction for sensor data. As summarized in Table 1, features are manually extracted from multiple sensors, including ram position, acceleration, force signals, and frame position. For ram position, piezo force, and frame position, the signals from the four sensors belonging to the same category are jointly modeled using a covariance matrix, which captures both the individual variances and the inter-sensor correlations over time, resulting in a 10-dimensional original feature

representation. In each experiment, the four resulting signal curves are assembled into a data matrix **D**.

$$\text{data} = \begin{bmatrix} x_1(1) & x_1(2) & \dots & x_1(N) \\ x_2(1) & x_2(2) & \dots & x_2(N) \\ x_3(1) & x_3(2) & \dots & x_3(N) \\ x_4(1) & x_4(2) & \dots & x_4(N) \end{bmatrix} \tag{3}$$

where x_k denotes four curves and $x_k(N)$ denotes the k-th point on the corresponding curve. The covariance matrix $\boldsymbol{C}$ is calculated by

$$\boldsymbol{C} = \frac{1}{N-1}(\boldsymbol{D} - \mu)(\boldsymbol{D} - \mu)^T, \tag{4}$$

where μ is the mean value of each row of **D**. This yields a 4×4 symmetric covariance matrix with 10 unique components. These 10 components can be vectorized and used as statistical features describing the ram position, piezo force, and frame position signals. These features include the correlations between sensors, such as $cov(x_1, x_2)$, as well as the fluctuation magnitude of each individual sensor, such as $cov(x_1, x_1)$.

For acceleration and ram force signals, statistical descriptors such as mean value, maximum value, standard deviation, frequency-domain mean, as well as displacement- and force-related maxima are extracted, yielding 4-dimensional original features. Let $\boldsymbol{x} = [x(1), x(2) \dots, x(K)]$ store the corresponding sensor data. For the feature extraction of acceleration signals, following formulas are used:

$$\max(x) = \max x(i), 1 \le i \le N, \tag{5}$$

$$\mu = \frac{1}{N}\sum_{i=1}^{N} x(i), \tag{6}$$

$$std(x) = \sqrt{\frac{1}{N-1}\sum_{i=1}^{N}(x(i) - \mu)^2}, \tag{7}$$

and the spectral energy feature is obtained by summing the squared FFT magnitudes

$$E = \sum_{k=0}^{N-1} |X[k]|^2, \tag{8}$$

where $X[k] = \sum_{i=1}^{N} x(i)e^{-j2\pi ki/N}$.

For the feature extraction of ram force signals, the position-force signal $\boldsymbol{f} = [f(p1), f(p2) \dots f(pN)]$ was considered. The following formulas are supplemented:

$$p_{F\_max} = \arg\max f(pi), 1 \le i \le N, \tag{9}$$

$$\frac{A}{\Delta x} = \frac{1}{\Delta x}\int f(x)dx, \tag{10}$$

where A denotes the area under the position-force curve within a displacement of Δx.

For the feature extraction of the radar data, the rear-left radar is taken as an example. Based on the time–frequency representation in Figure 6, a, we accumulate the spectral energy over the time interval from 0.4 s to 0.6 s at each frequency f, resulting in the frequency-dependent accumulated power spectrum $P_{acc}(f)$, as illustrated in Figure 6, b. This accumulated spectrum reflects

the dominant propagation paths as well as multipath components. The computation can be expressed as follows:

$$P_{acc}(f) = \sum_{t=t_1}^{t_2} P(f,t) \tag{11}$$

As shown in Figure 6, b, eight features are obtained by selecting the four highest spectral peaks from each side of the symmetric frequency range, which represent the dominant radar propagation paths.

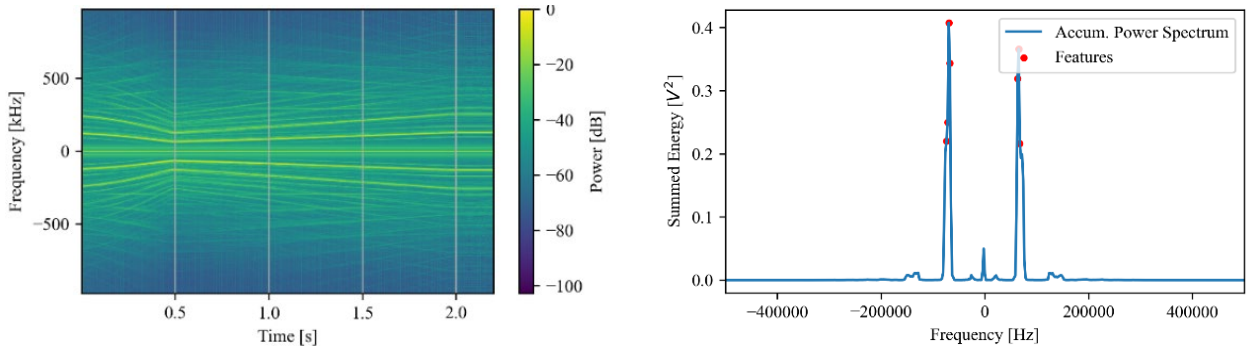

(a) (b)

Fig. 6. Example of accumulated radar frequency spectrum from 0.4 to 0.6 seconds. (a) Spectrogram of the FMCW radar (rear left), (b) Accumulated Power Spectrum of the FMCW radar(rear-left) from 0.4 to 0.6 seconds

Subsequently, LDA was applied to compress the manually extracted features of each type of sensor data into two discriminative components, leading to a consistent 2-dimensional representation per each type of sensor data (Table 4).

Table 4. Feature extraction for sensor data and LDA-compressed feature space

Sensor	**Manually extracted Features**	**Original feature number**	**LDA-compressed feature number (LDAs)**
Ram position	Covariance	10	2
Acceleration	Mean, maximum value, standard deviation, and FFT magnitude.	4	2
Force (Piezo)	Covariance	10	2
Force (Ram)	F_max, Area/Δx, standard deviation, p_{F_max}	4	2
Frame position	Covariance	10	2
Radar rear-left	Spectral peaks	8	2

Results and Discussion

Defect detection using feature extraction and LDA dimensionality reduction. The results of the LDA (Figure 7) show that the sensor data from defective and non-defective states can be separated to varying degrees depending on the sensor type. In particular, for the position sensors, PiezoBolts, radar sensors, and acceleration sensors, a clear shift of the projection distributions in the LDA projection space can be observed. This indicates a relevant dependency of the sensor signals on workpiece misalignment and thus on the occurrence of defects. Overall, the observed separability suggests that selected sensor data and process parameters contain relevant information for distinguishing between defect and non-defect states and can therefore be considered suitable input variables for subsequent data-driven models. It is noteworthy that even the features extracted from a single radar sensor already allow for an effective separation of the different states.

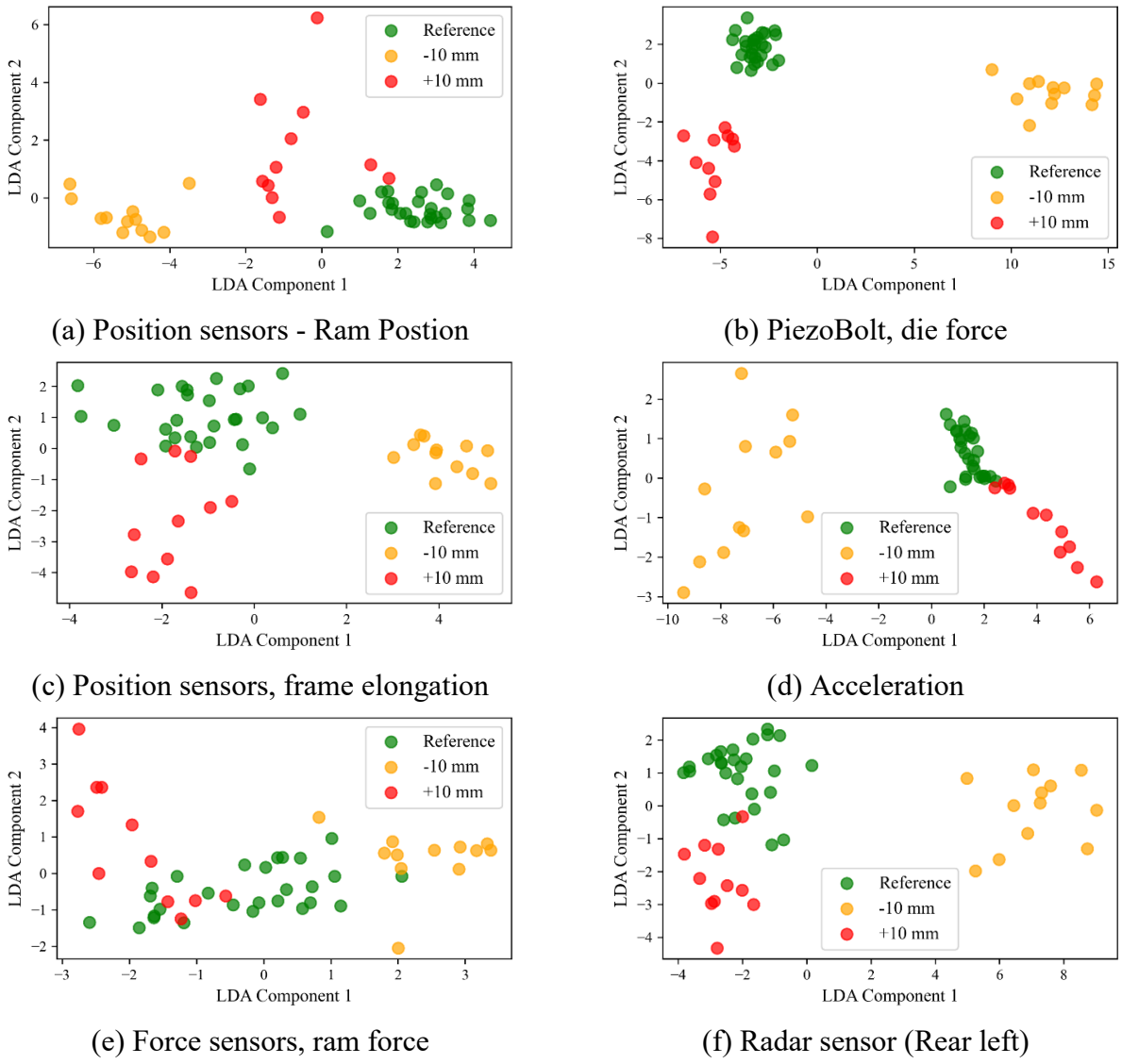

(a) Position sensors - Ram Postion

(b) PiezoBolt, die force

(c) Position sensors, frame elongation

(d) Acceleration

(e) Force sensors, ram force

(f) Radar sensor (Rear left)

Fig. 7. The results of the LDA

Forging machine behavior analysis. Based on experimental data the press frame deflection (Figure **8**, a) and the press ram tilting (Figure 8, b) were calculated.

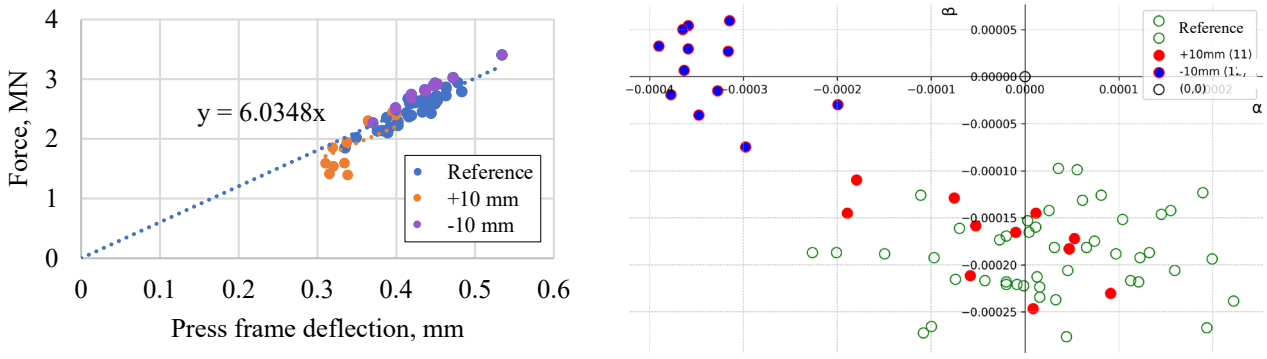

(a)

(b)

Fig.8. Press frame deflection (a) and press ram tilting (b) (α – in YOZ, β – in XOZ)

An average press frame stiffness of 6,03 MN/mm was calculated from the press frame deflection data. The maximum tilt angle of the press ram does not exceed 0.0005°.

Air entrapment in die cavities. Experimental data showed that even with reference process parameters, underfilling defects formed, although the simulation without considering air entrapment

predicted no defects (Figure 9). The simulation using the brand-new feature of QForm UK 12.0.1 predicted a formation of trapped air pockets, which led to the defect formation with biggest underfilling of 0.54 mm. The maximum pressure of the trapped air reached 202 MPa.

Description	Top view	Bottom view
Forged part		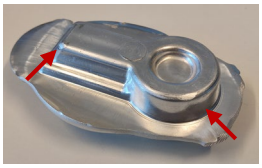
Distance to contact, mm Without air entrapment simulation	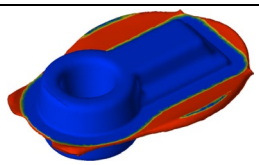	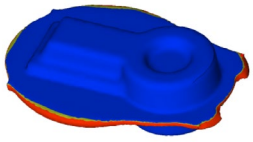
Distance to contact, mm With air entrapment simulation	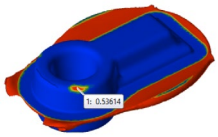	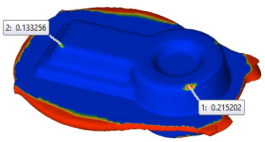
Trapped air pressure, MPa		

Fig. 9. Defect formation during forging without air vents

For a free venting of air from the die cavities, holes with a diameter of 0.5 mm were produced using electrical discharging (Figure 10).

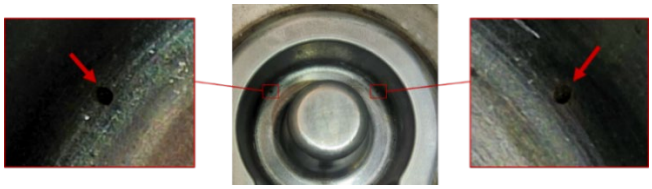

Fig.10. Air vent channels

The presence of holes allows air to leave the deep cavities of the die and prevents the formation of defects, which is also confirmed by simulations considering air entrapment (Figure 11).

Description	Top view	Bottom view
Forged part		
Contact areas	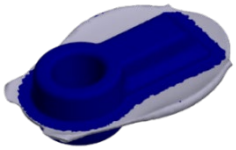	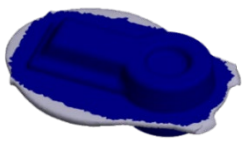

Fig. 11. No defects were observed during forging with air vents

FEM-dataset analysis using Random Forest. The $N_{pars} = 6$ input parameters of the FEM simulation were considered as features. The label was defined as a binary variable: samples with a distance between the forged workpiece boundary and the upper die exceeding 0.5 mm were labeled as 1 (defective), and those not exceeding this threshold were labeled as 0 (non-defective). A dataset

containing $N_{ins} = 120$ instances was generated using the Latin Hypercube Sampling within the range of the feature space, including $N_{d,ins} = 89$ cases with underfill and $N_{nd,ins} = 31$ free of underfill. The best estimator $[n_{estimators} = 100, max_{depth} = 15, min_{samples_{leaf}} = 1, min_{samples_{split}} = 15, class\ weight = 'balanced']$ with the 0.87 test accuracy was found using grid search method. For class 0, the recall is 0.83 and the F1-score is 0.77. For class 1, the recall reaches 0.89 with an F1-score of 0.91. The feature importance shown in Figure 12 were extracted.

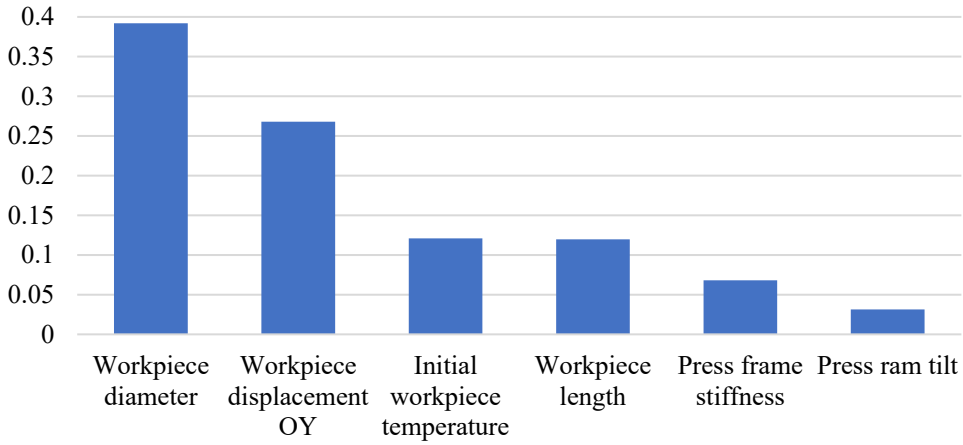

Fig. 12. Feature importance

To assess the robustness of the model performance, a Random Forest classifier was trained and evaluated using a systematic hyperparameter optimization combined with cross-validation. The model hyperparameters, including the number of trees, tree depth, and node regularization parameters, were optimized using a grid search with 10-fold cross-validation. The use of 10-fold cross-validation ensures that the reported performance is not dependent on a specific train–test split, as each sample is used for validation exactly once. In addition, the Random Forest model inherently improves robustness through bootstrap aggregation, where each tree is trained on a different bootstrap sample of the data. This ensemble strategy reduces sensitivity to individual samples and mitigates overfitting effects, and is particularly important in small-sample scenarios.

The stability of the reported feature importance results is supported by the use of cross-validation and ensemble learning. Since the Random Forest model is trained across multiple folds and hyperparameter configurations, the dominant features consistently emerged as important, while variations mainly affected lower-ranked features. Moreover, the use of balanced class weights was evaluated to account for potential label imbalance, ensuring that the learned model does not rely on the majority class.

Overall, the combination of ensemble learning, cross-validation-based hyperparameter tuning, and regularization results in a robust model whose performance and conclusions are not driven by individual samples or specific parameter choices. Nevertheless, we acknowledge that the generalizability of the model is currently limited to the parameter ranges covered by the FEM simulations. Future work will therefore focus on extending the dataset and integrating experimental data to further improve robustness.

The SHAP analysis is shown in Figure 13.

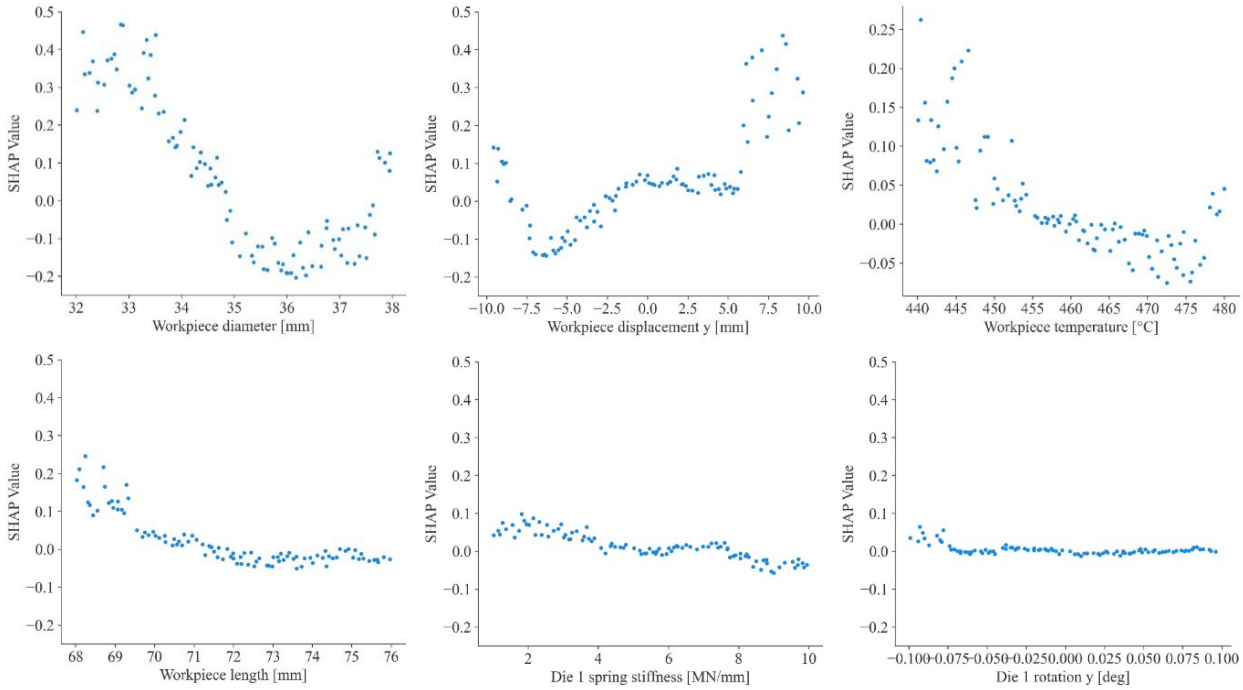

Fig. 13. SHAP analysis

As it can be seen, the workpiece diameter has a high impact on the defect formation. When it in the range between 35 mm and 37 mm, no defect was predicted. The workpiece diameter less than 35 mm leads to leak of metal, and therefore, to defect formation. Deviation of the workpiece position within ±5 mm can be can be assessed as safe, while a larger displacement of the workpiece leads to the formation of a defect. Reducing the initial workpiece temperature down to 460°C does not result in a defect. Reducing the workpiece length to 70 mm does not lead to defect formation, thus the process reference parameters can be improved. The press frame stiffness does not have a significant effect on defect formation, however, with press stiffness less than 6 MN/mm the probability of defect formation is slightly increased. The press ram tilt also has little effect on defect formation and the probability of defect formation increases only from a tilt of -0.075°, resulting in a lack of metal to form the forging head. As can be seen from the Figure 8, the actual press characteristics are such that they have no influence on the defect formation.

Conclusions

This work demonstrates that combining FEM simulations with data-driven modelling significantly improves the prediction and the detection of underfilling defects in hot forging. By integrating real-process effects, such as ram tilt, press-frame deflection and air entrapment, into the FEM model and complementing it with a sensor-based classification model, the hybrid framework captured defect-formation more accurately than either approach alone. The results highlight the value of hybrid numerical–data-driven strategies for enhancing the robustness and reliability of metal-forming process design.

Acknowledgment

This work was carried out in the framework of the project “DatProForge - Data-driven process modelling of closed-die forging processes to increase productivity using adaptive tool design methodology”, part of the DFG priority program “Data-driven process modelling in metal forming technology” (SPP 2422).

Funded by the Deutsche Forschungsgemeinschaft (DFG, German Research Foundation) – Project number 520194997.

References

[1] J. Chenot, E. Massoni, Jl. Fourment, Inverse problems in finite element simulation of metal forming processes, Eng. Comput. 13 (1996) 190–225. https://doi.org/10.1108/02644409610114530.

[2] J.-L. Chenot, M. Bernacki, P.-O. Bouchard, L. Fourment, E. Hachem, E. Perchat, Recent and future developments in finite element metal forming simulation, in:11th Int. Conf. Technol. Plast. ICTP 2014, 2014.

[3] L.C. Sousa, C.F. Castro, C.A.C. António, A.D. Santos, Inverse methods in design of industrial forging processes, J. Mater. Process. Technol. 128 (2002) 266–273. https://doi.org/10.1016/S0924-0136(02)00464-8.

[4] A. Andrade-Campos, S. Coppieters, M. Strano, Optimization and inverse analysis in metal forming: scientific state-of-the-art and recent trends, Int. J. Mater. Form. 15 (2022) 44. https://doi.org/10.1007/s12289-022-01690-8.

[5] W.L. Oberkampf, S.M. DeLand, B.M. Rutherford, K.V. Diegert, K.F. Alvin, Error and uncertainty in modeling and simulation, Reliab. Eng. Syst. Saf. 75 (2002) 333–357. https://doi.org/10.1016/S0951-8320(01)00120-X.

[6] M. Liewald, B. Vogel-Heuser, T. Bergs, M. Huber, P. Kröger, Advancing data-driven process modeling in metal forming, - Autom. 73 (2025) 162–173. https://doi.org/10.1515/auto-2024-0118.

[7] H. Song, C. Durand, C. Baudouin, R. Bigot, Dynamic modelling and efficiency prediction for forging operations under a screw press, Int. J. Adv. Manuf. Technol. 134 (2024) 645–656. https://doi.org/10.1007/s00170-024-14145-y.

[8] D. Uribe, C. Durand, C. Baudouin, R. Bigot, Accurate real-time modeling for multiple-blow forging, Int. J. Mater. Form. 17 (2024) 57. https://doi.org/10.1007/s12289-024-01861-9.

[9] Y. Jiang, M. Knaack, C.A. Martin, F. Tost, A. Alimov, S. Härtel, M. Gardill, A 120 GHz Industrial Radar Sensor Network for Condition Monitoring of a Forging Process, IEEE Sens. J. (2025) 1–1. https://doi.org/10.1109/JSEN.2025.3636060.

[10] M. Liewald, T. Bergs, P. Groche, B.-A. Behrens, D. Briesenick, M. Müller, P. Niemietz, C. Kubik, F. Müller, Perspectives on data-driven models and its potentials in metal forming and blanking technologies, Prod. Eng. 16 (2022) 607–625. https://doi.org/10.1007/s11740-022-01115-0.

[11] T.-L. Wu, Y.-C. Hwang, W.-X. Zhang, Machine learning-based model for detecting uneven wear and temperature deviation events in hot forging process, Int. J. Adv. Manuf. Technol. 119 (2022) 2743–2761. https://doi.org/10.1007/s00170-021-08256-z.

[12] A. Alimov, Y. Jiang, M. Gardill, S. Härtel, Integrating stochastic effects and uncertainties into inverse analysis of hot bulk forging processes through automated API-driven finite element simulations and machine learning, Mater. Res. Proc. 54 (2025).

[13] S. Kasilingam, R. Yang, S.K. Singh, M.A. Farahani, R. Rai, T. Wuest, Physics-based and data-driven hybrid modeling in manufacturing: a review, Prod. Manuf. Res. 12 (2024) 2305358. https://doi.org/10.1080/21693277.2024.2305358.

[14] C. Van Tyne, J. Walters, Understanding geometrical forging defects, Forge 8 (2007) 1–5.

[15] M. Hawryluk, S. Polak, M. Rychlik, Ł. Dudkiewicz, J. Borowski, M. Suliga, Possibilities of Measuring and Detecting Defects of Forged Parts in Die Hot-Forging Processes, Materials 17 (2023) 213. https://doi.org/10.3390/ma17010213.

[16] A. Alimov, D. Gerasimov, I. Medvedko, N. Biba, S. Härtel, Automated FEM-Based Optimization of Gas-Vent Channel Positioning in Hot-Forging Dies to Prevent Underfill Defects, in: Metalforming, Palermo, Italy, September 22-25, 2026.

[17] Y. Jiang, A. Alimov, M. Knaack, S. Härtel, M. Gardill, Data-driven approaches for predicting underfill in hot bulk forging processes, Mater. Res. Proc. 54 (2025).

[18] H. Gao, J.W. Davis, Why direct LDA is not equivalent to LDA, Pattern Recognit. 39 (2006) 1002–1006.

[19] A.R. Webb, Statistical pattern recognition, John Wiley & Sons, 2003.

[20] J.-S. Chou, T.-K. Nguyen, Forward forecast of stock price using sliding-window metaheuristic-optimized machine-learning regression, IEEE Trans. Ind. Inform. 14 (2018) 3132–3142.

[21] R. Al Mallah, A. Quintero, B. Farooq, Cooperative evaluation of the cause of urban traffic congestion via connected vehicles, IEEE Trans. Intell. Transp. Syst. 21 (2019) 59–67.

[22] A. Benouareth, An efficient face recognition approach combining likelihood-based sufficient dimension reduction and LDA, Multimed. Tools Appl. 80 (2021) 1457–1486.